arXiv:1612.03666v1 [math-ph] 12 Dec 2016

Conserved Currents in the Six-Vertex and Trigonometric Solid-On-Solid Models

Yacine Ikhlef*[1,2] and Robert Weston†[3]

[1]Sorbonne Universités, UPMC Univ Paris 06, UMR 7589, LPTHE, F-75005, Paris, France

[2]CNRS, UMR 7589, LPTHE, F-75005, Paris, France

[3]Department of Mathematics, Heriot-Watt University, Edinburgh EH14 4AS, UK, and Maxwell Institute for Mathematical Sciences, Edinburgh, UK

Dec. 12th, 2016

Abstract

We construct quasi-local conserved currents in the six-vertex model with anisotropy parameter η by making use of the quantum-group approach of Bernard and Felder. From these currents, we construct parafermionic operators with spin $1+i\eta/\pi$ that obey a discrete-integral condition around lattice plaquettes embedded into the complex plane. These operators are identified with primary fields in a $c=1$ compactified free Boson conformal field theory. We then consider a vertex-face correspondence that takes the six-vertex model to a trigonometric SOS model, and construct SOS operators that are the image of the six-vertex currents under this correspondence. We define corresponding SOS parafermionic operators with spins $s=1$ and $s=1+2i\eta/\pi$ that obey discrete integral conditions around SOS plaquettes embedded into the complex plane. We consider in detail the cyclic-SOS case corresponding to the choice $\eta=i\pi(p-p')/p$, with $p'<p$ coprime. We identify our SOS parafermionic operators in terms of the screening operators and primary fields of the associated $c=1-6(p-p')^2/pp'$ conformal field theory.

1 Introduction

Conserved currents play a key role in the construction and analysis of quantum field theories. They are of particular interest in two dimensions: using complex co-ordinates $z=x+it$ and $\bar{z}=x-it$, the current conservation law is

$$\partial_{\bar{z}}J-\partial_z\bar{J}=0\,, \tag{1.1}$$

and if the current obeys the additional condition

$$\partial_{\bar{z}}J+\partial_z\bar{J}=0\,, \tag{1.2}$$

then $\partial_{\bar{z}}J=0$ and so J is a holomorphic field – a hallmark of a conformal field theory (CFT).

Suppose we consider instead a two-dimensional classical statistical mechanical model which at a given critical point is expected to correspond to a specific CFT. These correspondences

*ikhlef@lpthe.jussieu.fr

†R.A.Weston@hw.ac.uk

are usually made by identifying critical indices, the central charge, finite-size behaviour, *etc.* Constructing and exploiting such connections has been one of the main activities and key successes of CFT since the earliest work [1]. While useful and exhaustive, most of the work that deals with the critical continuum limit of 2D lattice models has been heuristic. Rigorous results exist only for a very restricted set of solvable models: dimers [2] , the Ising model [3, 4], critical percolation [5, 6], and self-avoiding walks [7]. A necessary requirement for the proof of theorems relating to the critical continuum limit has been the construction of an operator that obeys a discrete-lattice version of both conditions (1.1) and (1.2). Such lattice operators are variously referred to as 'discretely-holomorphic' or 'preholomorphic' (see the review [8] and references therein).

The search for discretely-holomorphic operators beyond the class of models related to the Ising model has led a number of authors to consider how such operators might be constructed for 2D solvable lattice models and their associated 1D quantum integrable systems [9–17]. A systematic method of constructing currents obeying a discrete analogue of (1.1) for solvable models defined in terms of an underlying quantum group was formulated in [18]. This approach leads naturally to quasi-local operators – meaning that the operators are associated with both a lattice insertion point and a path from this point to the lattice boundary. This quantum-group method has been previously exploited by the current authors and collaborators in order to construct quasi-local conserved currents for dense and dilute loop models [14] and for the chiral Potts model [15].

In general, the quasi-local conserved currents that come from the quantum-group approach do not, at least by construction, obey a discrete version of equation (1.2); thus, they are not discretely holomorphic and their existence does not immediately open the way for a rigorous proof of the critical CFT limit. Nevertheless they have other uses: their conformal spin naturally appears in a direct way (see for example (4.24) below), and thus a heuristic identification with a CFT operator is almost immediate. Another, more formal, result is that the direct hexagonal-lattice analogue of the dense-loop-model operator was used in [7] in the proof of a long-standing conjecture of Nienhuis regarding the connectivity constant of a hexagonal lattice [19, 20]. A further example appeared in the context of the chiral Potts model in which the use of quantum group currents led to the definition of new parafermionic operators that generalise the parafermionic algebra of the $\mathbb{Z}_N$ clock model (which corresponds to the critical limit of the chiral Potts model) [15]. Furthermore, a careful analysis of the critical limit of the discrete version of (1.1) led to a perturbed CFT identification of the chiral Potts model that agreed with and extended a long-standing prediction of Cardy [21].

Motivated primarily by such practical uses, we describe in this paper the construction and CFT identification of conserved currents in the six-vertex (6V) model and a related trigonometric Solid-On-Solid (SOS) model. In the 6V model, these currents can be read off directly from the construction method of [18]. By identifying the spin in the manner mentioned above, we connect the critical continuum limit of these operators with primary fields in a compactified free-boson CFT. In contrast, such a direct approach is not possible for the trigonometric SOS model, as in this case there is no underlying quantum group (there *is* a quasi-Hopf algebra [22], but this algebra lacks the required coalgebra structure that is central to the approach of [18]). Instead, we rely on a vertex-face correspondence to map the currents of the 6V model to those of the SOS model. Given the quasi-local structure of the currents, it is by no means clear in advance that this mapping will lead to quasi-local operators in the SOS model, or that they will obey a discrete version of (1.1). We show that both of these statements are true and go on to identify the operators in different CFT limits.

The content of this paper is as follows: in Section 2 we give a brief description of discrete versions of the Cauchy-Riemann relations. Then in Section 3 we fix our conventions for the 6V and trigonometric SOS models, and give the vertex-face correspondence. In Section 4, we describe the construction of conserved currents within the algebraic picture of the 6V model, and

identify the resulting parafermionic operators with primary fields of a compactified free boson CFT in the critical continuum limit. In Section 5, we map the 6V currents to SOS currents using the vertex-face correspondence, and define parafermionic operators in the SOS model. We then consider the special case of cyclic SOS models in Section 6, and describe the identification of our lattice operators with local and parafermionic operators in CFT. Finally, we draw some conclusions in Section 7.

2 Discrete Current Conservation and Cauchy-Riemann Relations

In this section, we explain the various forms of the discrete relations that we refer to in the rest of the paper. The Cauchy-Riemann relations for a complex function $J_x(x,t) + iJ_t(x,t)$ are

$$\partial_t J_t - \partial_x J_x = 0\,, \tag{2.1}$$
$$\partial_x J_t + \partial_t J_x = 0\,. \tag{2.2}$$

Now consider a discretization of the above, where the functions are defined at the midpoints of a square unit-length lattice. More precisely, J_x will be defined on horizontal edges only, and J_t on vertical edges only. Then a possible discretization of these conditions is

$$J_t(\vec{u}_1) + J_x(\vec{u}_2) - J_t(\vec{u}_3) - J_x(\vec{u}_4) = 0\,, \tag{2.3}$$
$$J_x(\vec{v}_1) - J_t(\vec{v}_2) - J_x(\vec{v}_3) + J_t(\vec{v}_4) = 0\,, \tag{2.4}$$

around the following plaquettes:

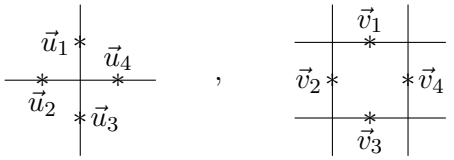

(2.5)

We can embed these relations into the complex plane in various ways. The obvious way is to choose the embedding $\iota : (x,t) \mapsto x + it$. Then defining

$$\Phi(x+it) = \begin{cases} J_x(x,t), & \text{if } (x,t) \text{ is a horizontal edge,} \\ iJ_t(x,t), & \text{if } (x,t) \text{ is a vertical edge,} \end{cases}$$

we see that the relations (2.3–2.4) become respectively

$$\sum_{i=1}^{4} \Phi(z_i)\delta z_i = 0, \qquad \sum_{i=1}^{4} \Phi(w_i)\delta w_i = 0\,, \tag{2.6}$$

where $z_i = \iota(\vec{u}_i)$, $w_i = \iota(\vec{v}_i)$, and δz_i and δw_i are the anticlockwise oriented edges of the embedded plaquettes corresponding to (2.5). At this point, it is important to point out a potential source of confusion: we use the notation $\Phi(z)$ for this and other discrete functions in the complex plane (as opposed to, say, $\Phi(z,\bar{z})$) but this does *not* imply that Φ is a holomorphic, or discretely holomorphic, function.

A more general embedding is $\iota : (x,t) \mapsto e^{i\alpha_1}x + e^{i\alpha_2}t$, where α_1 and α_2 are the angles of the images of the x and t axes in the complex plane. Then we define

$$\Phi(e^{i\alpha_1}x + e^{i\alpha_2}t) = \begin{cases} e^{i\alpha_1}J_x(x,t), & \text{if } (x,t) \text{ is a horizontal edge,} \\ e^{i\alpha_2}J_t(x,t), & \text{if } (x,t) \text{ is a vertical edge,} \end{cases}$$

The relations (2.6) still follow from the discrete relations (2.3–2.4) in this more general case. The sums in (2.6) may be interpreted as discrete integrals around the corresponding embedded rhombic plaquettes.

Thus, starting from just a current conservation law of the form (2.3), we have different ways of choosing the embedding into the complex plane to obtain a discrete integral condition $\sum_{i=1}^{4} \Phi(z_i)\delta z_i = 0$ around a vertex. In the following sections, we shall use a particular embedding, whose choice is determined by consistency with the Yang-Baxter equation and crossing symmetry, and which produces an operator $\Phi(z)$ in a simple form with a prefactor that can be immediately interpreted in terms of the spin of the operator.

3 The Six-Vertex and Trigonometric SOS Models

In this section, we introduce our notation for the six-vertex model and describe a vertex-face correspondence between the Boltzmann weights of this model and those of a trigonometric SOS model. Our prescription is a trigonometric limit of the standard vertex-face correspondence between the eight-vertex and elliptic SOS models described in [23, 24]. We were inspired to consider such trigonometric SOS models by the work [25]. We will firstly recall how the partition function of both models are related under the vertex-face correspondence. Then in Section 5, we will go on to consider how correlation functions of our quasi-local operators behave under the vertex-face correspondence.

3.1 The six-vertex model

We consider the six-vertex model with Boltzmann weights parametrized as

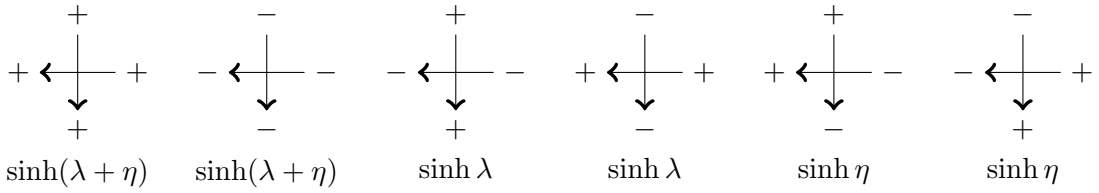

where λ and η are complex numbers. Note that we use $\pm$ for the spin variables, while the arrows indicate the orientation of the lines of the lattice. The weights corresponding to the above vertices form the entries of the R-matrix

$$R(\lambda)^{\varepsilon_1,\varepsilon_2}_{\varepsilon_1',\varepsilon_2'} =$$

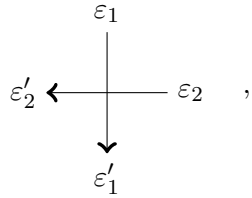

,

and it is sometimes useful to associate the spectral parameter λ with the edges as follows:

$$R(\lambda_1-\lambda_2)^{\varepsilon_1,\varepsilon_2}_{\varepsilon_1',\varepsilon_2'} =$$

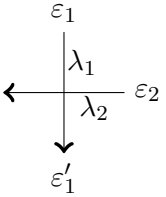

.

In matrix-form we have

$$R(\lambda) = \begin{pmatrix} \sinh(\lambda+\eta) & 0 & 0 & 0 \\ 0 & \sinh\lambda & \sinh\eta & 0 \\ 0 & \sinh\eta & \sinh\lambda & 0 \\ 0 & 0 & 0 & \sinh(\lambda+\eta) \end{pmatrix} . \tag{3.1}$$

The R-matrix obeys the Yang-Baxter equation

$$R_{12}(\lambda_1-\lambda_2)R_{13}(\lambda_1-\lambda_3)R_{23}(\lambda_2-\lambda_3) = R_{23}(\lambda_2-\lambda_3)R_{13}(\lambda_1-\lambda_3)R_{12}(\lambda_1-\lambda_2)\,, \tag{3.2}$$

which can be represented as:

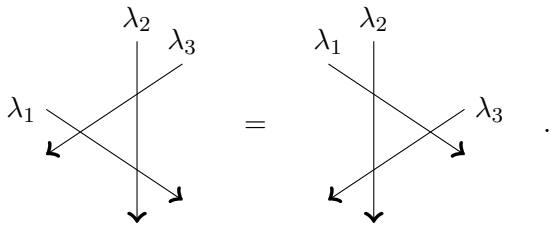

The R-matrix also satisfies the (normalised) unitarity and crossing symmetry relations

$$R_{21}(-\lambda)R_{12}(\lambda) = \sinh(\lambda+\eta)\sinh(-\lambda+\eta)\;\mathbb{1}\,, \tag{3.3}$$

$$R(\lambda)^{\varepsilon_1,\varepsilon_2}_{\varepsilon_1',\varepsilon_2'} = (-1)^{\frac{\varepsilon_1+\varepsilon_1'}{2}} R(-\lambda-\eta)^{\varepsilon_2,-\varepsilon_1'}_{\varepsilon_2',-\varepsilon_1}\,. \tag{3.4}$$

3.2 The trigonometric SOS model

Baxter showed in [23] that it was possible to relate the eight-vertex model to an elliptic SOS model – the latter is a height model on a square lattice with Boltzmann weights associated with the faces. This correspondence was generalised in subsequent work [26] and also re-expressed in the language of the dynamical Yang-Baxter equation [27]. We do not need or discuss this dynamical approach in this paper.

3.2.1 The vertex-face correspondence

The starting point for our trigonometric vertex-face correspondence is to introduce certain vector-valued functions of the spectral parameter λ that depend upon pairs (a,b) of *height variables* living in $x_0+\mathbb{Z}$ (where $x_0\in\mathbb{C}$ is an arbitrary reference point) with $|a-b|=1$. These functions are sometimes called *Baxter intertwiners*. More precisely, we have a column-vector valued function $\psi(a,b|\lambda)$ and row-vector valued function $\psi^*(a,b|\lambda)$ given by

$$\psi(a,a\pm1|\lambda) = \begin{bmatrix} \exp\left(\frac{-\lambda\pm a\eta}{2}\right) \\ \exp\left(\frac{+\lambda\mp a\eta}{2}\right) \end{bmatrix}\,, \tag{3.5}$$

$$\psi^*(a,a\pm1|\lambda) = \frac{\pm1}{2\sinh a\eta}\left[\exp\left(\frac{+\lambda\pm a\eta}{2}\right)\,,\quad -\exp\left(\frac{-\lambda\mp a\eta}{2}\right)\right]. \tag{3.6}$$

The following pictorial representation [28] of the vector components $\psi(a,b|\lambda)_\varepsilon$, $\psi^*(a,b|\lambda)_\varepsilon$, $\varepsilon\in\{\pm1\}$, is very useful:

$\psi(a,b|\lambda)_\varepsilon =$ 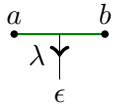

, $\psi^*(a,b|\lambda)_\varepsilon =$ 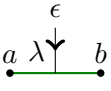

.

The six-vertex R-matrix and Baxter intertwiners obey the following relations

$$R(\lambda_{12})\,[\psi(a,b|\lambda_1)\otimes\psi(b,c|\lambda_2)] = \sum_d [\psi(d,c|\lambda_1)\otimes\psi(a,d|\lambda_2)]\;\; W\left(\begin{array}{cc} a & b \\ d & c \end{array}\middle|\,\lambda_{12}\right)\,, \tag{3.7}$$

$$[\psi^*(d,c|\lambda_1)\otimes\psi^*(a,d|\lambda_2)]R(\lambda_{12}) = \sum_b W\left(\begin{array}{cc} a & b \\ d & c \end{array}\middle|\,\lambda_{12}\right)[\psi^*(a,b|\lambda_1)\otimes\psi^*(b,c|\lambda_2)]\,, \tag{3.8}$$

where we introduce the notation $\lambda_{ij} = \lambda_i - \lambda_j$. Here the function W depends on four height variables (a,b,c,d) and is non-zero in the case when $|a-b| = |b-c| = |c-d| = |d-a| = 1$. Explicitly, we have for any $a \in x_0 + \mathbb{Z}$

$$\begin{aligned} W\left(\begin{array}{cc} a & a\pm 1 \\ a\pm 1 & a\pm 2 \end{array}\middle|\,\lambda\right) &= \sinh(\lambda+\eta), \\ W\left(\begin{array}{cc} a & a\pm 1 \\ a\mp 1 & a \end{array}\middle|\,\lambda\right) &= \frac{\sinh\lambda\;\sinh[(a\pm 1)\eta]}{\sinh(a\eta)}, \\ W\left(\begin{array}{cc} a & a\pm 1 \\ a\pm 1 & a \end{array}\middle|\,\lambda\right) &= \frac{\sinh\eta\;\sinh(a\eta\mp\lambda)}{\sinh(a\eta)}. \end{aligned} \tag{3.9}$$

This function will form the Boltzmann weight of a configuration of four heights around a face, which we represent by the picture

$W\left(\begin{array}{cc} a & b \\ d & c \end{array}\middle|\,\lambda\right)$ =

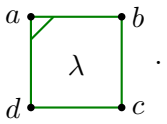

.

We refer to the statistical-mechanical model so-defined as the trigonometric SOS model (or just SOS model). With these graphical conventions, the vertex-face correspondence relations (3.7–3.8) become

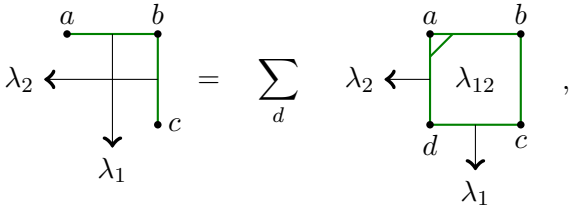

, (3.10)

and

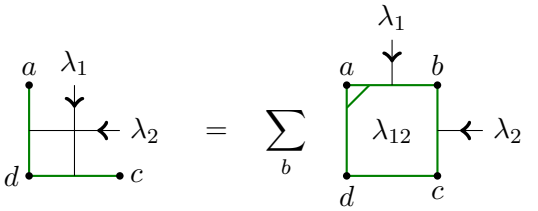

. (3.11)

The Baxter intertwiners ψ and ψ^* also obey the following inversion relations:

$$\psi^*(a,c|\lambda)\psi(a,b|\lambda) = \delta_{bc}\,, \tag{3.12a}$$

$$\sum_b \psi(a,b|\lambda)\psi^*(a,b|\lambda) = \mathbb{1}\,, \tag{3.12b}$$

$$\psi'(c,a|\lambda)\psi(b,a|\lambda) \;= \delta_{bc} \tag{3.12c}$$

$$\sum_b \psi(b,a|\lambda)\psi'(b,a|\lambda) = \mathbb{1}\,. \tag{3.12d}$$

where, following [28, 29], we define

$$\psi'(a,b|\lambda) = \frac{\sinh(a\eta)}{\sinh(b\eta)}\psi^*(a,b|\lambda)e^{\eta\sigma^z}.$$

If we represent this modified intertwiner as

$\psi'(a,b|\lambda) =$ 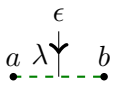

,

then the inversion relations (3.12) appear as

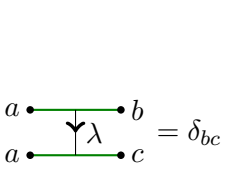

$= \delta_{bc}$

(a)

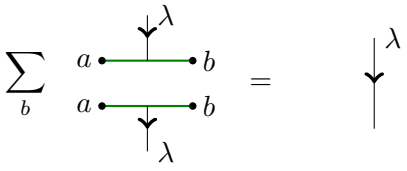

(b)

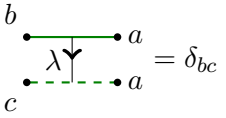

$= \delta_{bc}$

(c)

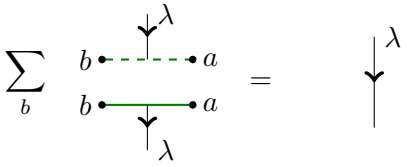

(d)

The SOS model weights obey the face version of the Yang-Baxter equation

$$\sum_g W\left(\begin{matrix} f & g \\ e & d \end{matrix}\middle|\lambda_{12}\right) W\left(\begin{matrix} a & b \\ f & g \end{matrix}\middle|\lambda_{13}\right) W\left(\begin{matrix} b & c \\ g & d \end{matrix}\middle|\lambda_{23}\right)$$
$$= \sum_g W\left(\begin{matrix} a & g \\ f & e \end{matrix}\middle|\lambda_{23}\right) W\left(\begin{matrix} g & c \\ e & d \end{matrix}\middle|\lambda_{13}\right) W\left(\begin{matrix} a & b \\ g & c \end{matrix}\middle|\lambda_{12}\right). \tag{3.13}$$

Graphically, this is represented as:

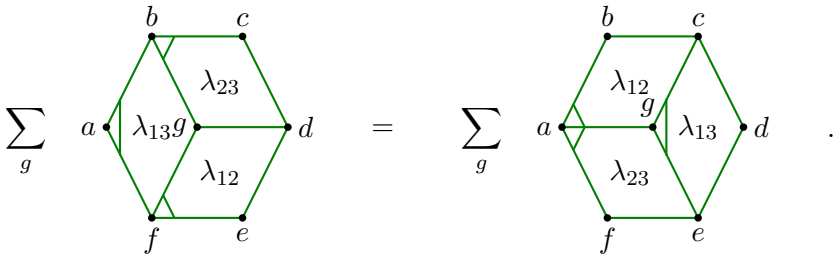

.

3.2.2 Correspondence of the partition functions

The correspondence between the partition functions of the six-vertex and SOS models starts by dressing the boundary of the six-vertex model with the Baxter intertwiners, with the external boundary heights fixed. The vertex-face correspondence is used repeatedly starting either from the NE or SW corner of the lattice. If we start from the NE corner and use (3.7) then we arrive

at the correspondence

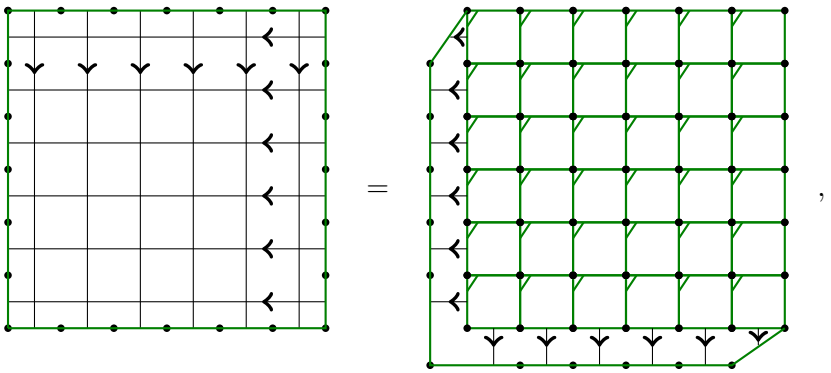

where all internal height variables are summed over. We can then apply the relation (3.12a) repeatedly starting from the NW corner, in order to arrive at equality with the pure SOS partition function:

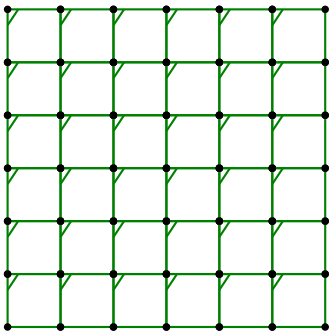

We can also apply this vertex-face correspondence to connect correlation functions of local operators in the six-vertex model to those in the SOS model. This approach was used successfully to compute such correlation functions in the eight-vertex case in the thermodynamic limit in [28, 29]. In this paper we are interested in using the vertex-face correspondence to connect correlation functions of *quasi-local* operators in the six-vertex and SOS models for finite-size lattices. We shall introduce the relevant six-vertex model quasi-local operators in the next section.

4 Conserved Currents in the Six-Vertex Model

In this section, we recall the relation of the six-vertex model to the quantum affine algebra $U_q(\widehat{\mathfrak{sl}}_2)$, and construct quasi-local conserved currents in terms of the Chevalley generators of this algebra. This way of relating quantum groups and quasi-local conserved currents was proposed in a more general setting by Bernard and Felder [18] and was exploited in the context of discrete holomorphicity in previous work of the authors and collaborators [14, 15].

4.1 The algebraic picture of the six-vertex model

The algebra $U_q(\widehat{\mathfrak{sl}}_2)$ is an associative algebra generated by the Chevalley generators $e_i, f_i, t_i^{\pm 1}$, $i \in \{0, 1\}$, with relations

$$t_i e_j t_i^{-1} = q^{A_{ij}} e_j \,, \quad t_i f_j t_i^{-1} = q^{-A_{ij}} f_j \,, \quad [e_i, f_j] = \delta_{i,j} \frac{t_i - t_i^{-1}}{q - q^{-1}} \,, \quad A = \begin{pmatrix} 2 & -2 \\ -2 & 2 \end{pmatrix} , \tag{4.1}$$

and additional Serre relations (a gentle introduction to quantum affine algebras can be found in [30]). Here q is a parameter, which we can take to be a complex number, and we write:

$$q = e^{\eta}\,.$$

The algebra is a Hopf algebra, meaning that it has additional structure including a coproduct $\Delta : U_q(\widehat{\mathfrak{sl}}_2) \to U_q(\widehat{\mathfrak{sl}}_2) \otimes U_q(\widehat{\mathfrak{sl}}_2)$ and an antipode $S : U_q(\widehat{\mathfrak{sl}}_2) \to U_q(\widehat{\mathfrak{sl}}_2)$, which we here choose as

$$\Delta(e_i) = e_i \otimes \mathbb{1} + t_i \otimes e_i\,, \qquad \Delta(f_i) = f_i \otimes t_i^{-1} + \mathbb{1} \otimes f_i\,, \qquad \Delta(t_i^{\pm 1}) = t_i^{\pm 1} \otimes t_i^{\pm 1}, \tag{4.2}$$

$$S(e_i) = -t_i^{-1} e_i\,, \qquad S(f_i) = -f_i t_i\,, \qquad S(t_i^{\pm 1}) = t_i^{\mp 1}\,. \tag{4.3}$$

The representation of $U_q(\widehat{\mathfrak{sl}}_2)$ that is relevant to the six-vertex model is that specified by the module $V_\lambda = \mathbb{C}^2 \otimes \mathbb{C}[e^\lambda, e^{-\lambda}]$ with action

$$\begin{aligned} e_1 &\mapsto \begin{pmatrix} 0 & e^{\lambda} \\ 0 & 0 \end{pmatrix}, \qquad f_1 \mapsto \begin{pmatrix} 0 & 0 \\ e^{-\lambda} & 0 \end{pmatrix}, \qquad t_1 \mapsto \begin{pmatrix} e^{\eta} & 0 \\ 0 & e^{-\eta} \end{pmatrix}, \\ e_0 &\mapsto \begin{pmatrix} 0 & 0 \\ e^{\lambda} & 0 \end{pmatrix}, \qquad f_0 \mapsto \begin{pmatrix} 0 & e^{-\lambda} \\ 0 & 0 \end{pmatrix}, \qquad t_0 \mapsto \begin{pmatrix} e^{-\eta} & 0 \\ 0 & e^{\eta} \end{pmatrix}. \end{aligned} \tag{4.4}$$

The R-matrix (3.1) is then the map

$$R(\lambda_1 - \lambda_2) : V_{\lambda_1} \otimes V_{\lambda_2} \to V_{\lambda_1} \otimes V_{\lambda_2}$$

such that, for any $x \in U_q(\widehat{\mathfrak{sl}}_2)$,

$$R(\lambda_1 - \lambda_2) \circ \Delta(x) = \Delta'(x) \circ R(\lambda_1 - \lambda_2)\,, \tag{4.5}$$

where $\Delta'(x) = P \circ \Delta(x) \circ P$ is the opposite co-product with $P(x \otimes y) = y \otimes x$.

4.2 Currents corresponding to Chevalley generators

For our purposes, it is useful to consider the generators $\bar{f}_i = e_i\, t_i^{-1}$ with

$$\Delta(\bar{f}_i) = \bar{f}_i \otimes t_i^{-1} + \mathbb{1} \otimes \bar{f}_j\,, \tag{4.6}$$

and

$$\bar{f}_1 \mapsto \begin{pmatrix} 0 & e^{\lambda+\eta} \\ 0 & 0 \end{pmatrix}, \quad \bar{f}_0 \mapsto \begin{pmatrix} 0 & 0 \\ e^{\lambda+\eta} & 0 \end{pmatrix}, \tag{4.7}$$

following from the above. The coproduct structure means that there is action of $U_q(\widehat{\mathfrak{sl}}_2)$ on the N-fold tensor product $V_\lambda^{\otimes N}$ given by the iterated coproduct $\Delta^{(N)} : U_q(\widehat{\mathfrak{sl}}_2) \to U_q(\widehat{\mathfrak{sl}}_2)^{\otimes N}$, with $\Delta^{(N)} = (\Delta \otimes \mathbb{1})\Delta^{(N-1)}$ and $\Delta^{(2)} = \Delta$. The action of f_i, $\bar{f}_i$ and t_i^{-1} on this space is given by

$$\begin{aligned} \Delta^{(N)}(f_i) &= \sum_{j=1}^{N} \mathbb{1} \otimes \mathbb{1} \otimes \cdots \underset{(j-\text{th})}{f_i} \cdots \otimes t_i^{-1} \otimes t_i^{-1} \otimes \cdots t_i^{-1}, \\ \Delta^{(N)}(\bar{f}_i) &= \sum_{j=1}^{N} \mathbb{1} \otimes \mathbb{1} \otimes \cdots \underset{(j-\text{th})}{\bar{f}_i} \cdots \otimes t_i^{-1} \otimes t_i^{-1} \otimes \cdots t_i^{-1}, \\ \Delta^{(N)}(t_i^{\pm 1}) &= t_i^{\pm 1} \otimes t_i^{\pm 1} \otimes \cdots \otimes t_i^{\pm 1} \otimes t_i^{\pm 1}. \end{aligned}$$

Now we adopt the pictorial representation of [18]: we represent the space V_λ by a downwards directed edge and the action of either f_i or $\bar{f}_i$ as[1]

$f_i, \bar{f}_i =$.

[1]We could distinguish the operators f_i or $\bar{f}_i$ pictorially by attaching a i or $\bar{i}$ index to the wavy line, but here we suppress this additional information in order to simplify the notation.

Furthermore, we represent the action of t_i and t_i^{-1} on V_λ by

$t_i =$, $t_i^{-1} =$.

The action of f_i or $\bar{f}_i$ on the space $V_\lambda^{\otimes N}$ can be represented by

$\sum_{j=1}^{N}$ 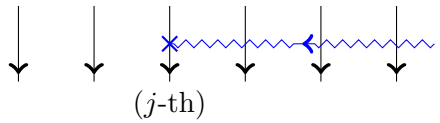

,

and the action of t_i and t_i^{-1} by

$t_i =$ 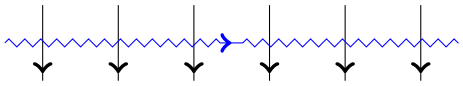 ,

$t_i^{-1} =$ 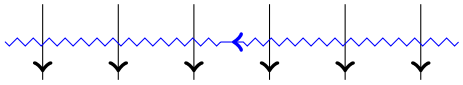 .

4.3 Elementary moves of tail operators

The (negative of) antipodes $-S(f_i) = f_i t_i =: \bar{e}_i$ and $-S(\bar{f}_i) = \bar{f}_i t_i = e_i$ then have the natural graphical realisation

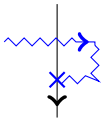 ,

which we can in turn abbreviate by

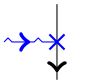 .

The relations $t_i f_i t_i^{-1} = e^{-2\eta} f_i$ and $t_i^{-1} f_i t_i = e^{2\eta} f_i$ (and similar relations with $f_i \to \bar{f}_i$), appear as the following:

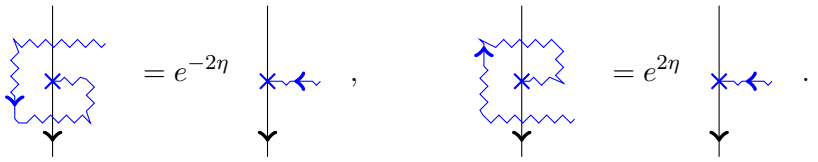

(4.8)

Finally, we note that $t_i^{-1} t_i = \mathbb{1} = t_i t_i^{-1}$ has the diagrammatic realisation

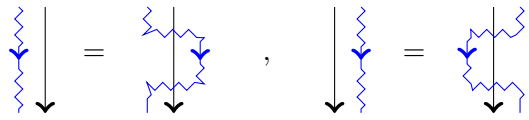

(4.9)

Using (4.5) with $x = t_i^{\pm 1}$ we have

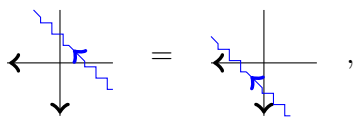

(4.10)

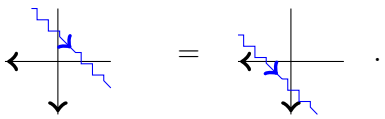

(4.11)

4.4 Current conservation

Now let us use the R-matrix commutation relation (4.5) with $x = f_i, \bar{f}_i$. Noting the coproduct formulae (4.2) and (4.6), it is apparent that this commutation relation becomes

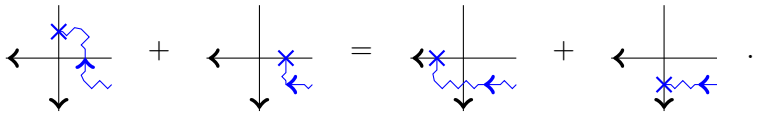

(4.12)

Hence, we have the four-term relation

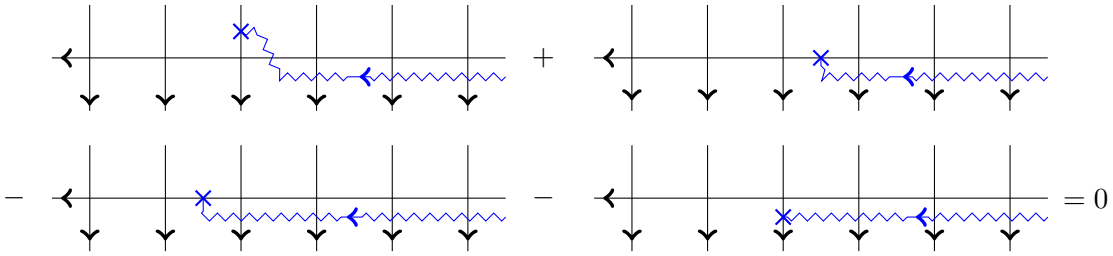

around any vertex (the third from the left in the example) in a product of R-matrices. Also note that using (4.10) and (4.11) one can move the wavy 'tail' corresponding to either t_i or t_i^{-1} through any vertex. Exploiting this ability we find for example that

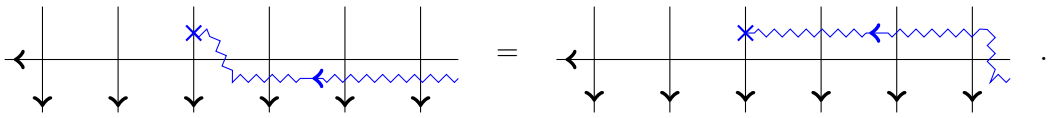

We can extend these various relations to the computation of correlation functions of these quasi-local operator insertions into the 2D lattice. For example we might compute the correlation function corresponding to the configuration sum with the following operator insertion at the lattice point $\vec{r}$ (corresponding to the cross):

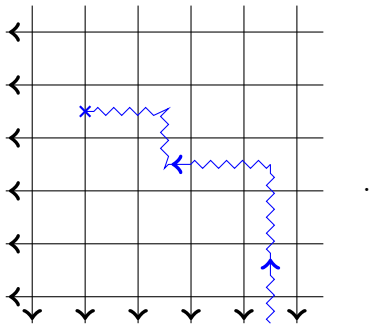

Dividing this configuration sum by the partition function, we obtain a quasi-local current expectation value, which we can denote by $\langle j(\vec{r})\rangle$. It will depend on the insertion point $\vec{r}$ and the boundary point (which we assume fixed), but not on the precise path followed by the tail – which can be moved according to (4.10–4.11). If we denote the four lattice insertion points around a vertex as $(\vec{r}_1, \vec{r}_2, \vec{r}_3, \vec{r}_4)$ corresponding to the picture

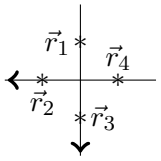

(4.13)

then the four-term relation discussed above will be of the form

$$j(\vec{r}_1) - j(\vec{r}_2) - j(\vec{r}_3) + j(\vec{r}_4) = 0\,, \tag{4.14}$$

where we have dropped the implied expectation values to simplify notation.

Suppose now that we have a quasi-local operator of the above form for which the tail has a non-zero winding number M around the insertion point. Using the relations (4.8), (4.10) and (4.11), we can 'unwind' the tail at the expense of picking up a factor $e^{-2\eta M}$.

4.5 Parafermionic operators

We now follow the procedure, outlined in Section 2, in which we embed the 2D lattice into the complex plane and interpret the relation (4.14) as a discrete integral condition around a rhombus[2]. We will embed the lattice into the plane so that the plaquette (4.13) becomes a unit rhombus with angle θ thus:

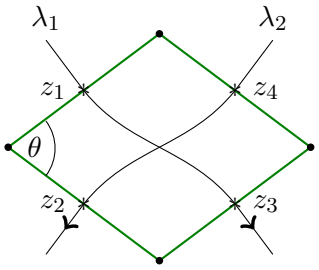

(4.15)

where $z_i \in \mathbb{C}$ denotes the image of $\vec{r}_i$. This embedding is achieved by mapping a line with spectral parameter λ to a line in the complex plane characterised by the angle α defined by

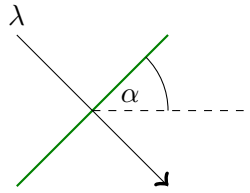

, (4.16)

where the green and black lines meet at 90 degrees, and in which α is specified in terms of λ by the relation

$$\alpha = -\frac{\pi\lambda}{\eta}\,. \tag{4.17}$$

With these conventions, we have that θ in (4.15) is given by

$$\theta = \alpha_1 - \alpha_2 = \frac{\pi(\lambda_2 - \lambda_1)}{\eta}. \tag{4.18}$$

which is consistent with both the Yang-Baxter relation (3.2) (interpreted as a geometrical relation in the plane) and the crossing relation (3.4) (interpreted as reversing the direction of a line). Note that in order that in order that the intersection point of black and green lines occurs at the midpoints of the edges of the rhombus, we need to distort the black lines as shown in (4.15).

We now need to introduce two more pieces of notation: firstly, we use $\alpha(z)$ to refer to the angle of the line passing through an embedded point z thus:

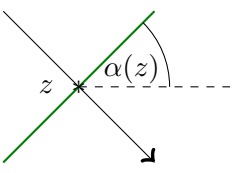

, (4.19)

[2]Note that there are slight modifications to the discussion in Section 2 resulting from the choice of orientation of our R-matrices.

Secondly, if we have a function $f : \mathbb{Z}^2 \to \mathbb{C}$, and an injection $\iota : \mathbb{Z}^2 \to \mathbb{C}$, then there is a unique map $F : \iota(\mathbb{Z}^2) \to \mathbb{C}$ defined by $F(\iota(\vec{r})) = f(\vec{r})$. At the potential risk of confusion we shall denote this map F by the same symbol $f(z)$ and refer to it as the image of $f(\vec{r})$, where $z = \iota(\vec{r})$.

We now wish to define an operator corresponding to the image of the different quasi-local operators $j(\vec{r})$ considered in Section 4.2. To this end, let us first refine the notation of Section 4.2: we use $j_i(\vec{r})$ to refer to the quasi-local operator associated with the generator f_i, and $\bar{j}_i(\vec{r})$ to refer to that associated with $\bar{f}_i$. Let us now modify $j_i(z)$ and $\bar{j}_i(z)$ (the images of $j_i(\vec{r})$ and $\bar{j}_i(\vec{r})$ under our embedding into the complex plane) in order to define operators $\phi_i(z)$ and $\bar{\phi}_i(z)$ as follows[3]

$$\phi_i(z) = e^{-i\alpha(z)} j_i(z)\,, \tag{4.20}$$

$$\bar{\phi}_i(z) = e^{+i\alpha(z)} \bar{j}_i(z)\,. \tag{4.21}$$

These operators obey the four-term relations

$$\delta z_1\, \phi_i(z_1) + \delta z_2\, \phi_i(z_2) + \delta z_3\, \phi_i(z_3) + \delta z_4\, \phi_i(z_4) = 0\,, \tag{4.22}$$

$$\overline{\delta z}_1\, \bar{\phi}_i(z_1) + \overline{\delta z}_2\, \bar{\phi}_i(z_2) + \overline{\delta z}_3\, \bar{\phi}_i(z_3) + \overline{\delta z}_4\, \bar{\phi}_i(z_4) = 0\,, \tag{4.23}$$

where δz_i refers to the complex number associated with the corresponding anti-clockwise plaquette edge in (4.15), and $\overline{\delta z}_i$ is its complex conjugate. As explained in Section 2, the first of these relations is a discrete integral condition around the embedded plaquette, corresponding to one half of the Cauchy-Riemann relations: it might be referred to as a half-discrete-holomorphicity condition. The second relation is similarly a discrete version of one half of the relations related to discrete-antiholomorphicity.

Let us now consider the spectral parameter dependence of the various currents. From the representation given by (4.4) and (4.7) it is clear that we can express

$$j_i(z) = e^{-\lambda(z)}\, \mathfrak{j}_i(z)\,,$$
$$\bar{j}_i(z) = e^{+\lambda(z)}\, \bar{\mathfrak{j}}_i(z)\,,$$

where the operators $\mathfrak{j}$ and $\bar{\mathfrak{j}}$ have no explicit spectral parameter dependence and are of the form

$$\mathfrak{j}_0(z) = \sigma^+(z) \otimes e^{\eta\sigma_3} \otimes e^{\eta\sigma_3} \otimes \cdots$$
$$\mathfrak{j}_1(z) = \sigma^-(z) \otimes e^{-\eta\sigma_3} \otimes e^{-\eta\sigma_3} \otimes \cdots$$
$$\bar{\mathfrak{j}}_0(z) = e^{\eta}\, \sigma^-(z) \otimes e^{\eta\sigma_3} \otimes e^{\eta\sigma_3} \otimes \cdots$$
$$\bar{\mathfrak{j}}_1(z) = e^{\eta}\, \sigma^+(z) \otimes e^{-\eta\sigma_3} \otimes e^{-\eta\sigma_3} \otimes \cdots$$

Noting the relation (4.17), it follows that we have

$$\phi_i(z) = e^{-is_i\alpha(z)}\, \mathfrak{j}_i(z)\,, \tag{4.24}$$

$$\bar{\phi}_i(z) = e^{+is_i\alpha(z)}\, \bar{\mathfrak{j}}_i(z)\,, \tag{4.25}$$

where all angular information is encoded in the 'spin' s_i defined as

$$s_0 = s_1 = 1 + \frac{i\eta}{\pi}\,. \tag{4.26}$$

Note that this is exactly the internal spin expected from the winding factors $e^{\pm 2\eta}$ in (4.8).

[3]Here and elsewhere in this paper i denotes $\sqrt{-1}$ when it does not appear as a subscript.

4.6 CFT interpretation

In the scaling limit, the critical 6V model is described by a compactified free boson action [31]:

$$\mathcal{A}[\varphi] = \frac{g}{4\pi}\int d^2r\,[\nabla\varphi(\vec{r})]^2\,, \qquad \varphi \equiv \varphi + 2\pi\,, \tag{4.27}$$

where $g = 1 + i\eta/\pi$. By convention, the bosonic field φ is the coarse-grained limit of a height variable defined on the dual lattice, with jumps $\pm\pi$ according to the sign of arrows in the 6V configuration. The central charge is $c = 1$. The primary operators in this theory are indexed by integer 'electric' and 'magnetic' charges (e, m), and have conformal dimensions:

$$\Delta_{e,m} = \frac{(e+mg)^2}{4g}\,, \qquad \bar{\Delta}_{e,m} = \frac{(e-mg)^2}{4g}\,. \tag{4.28}$$

More generally, the quasi-local operator inserting a tail of the form $e^{i\alpha\sigma_3}\otimes e^{i\alpha\sigma_3}\otimes\ldots$ corresponds to a non-integer electric charge $e \in \alpha/\pi + \mathbb{Z}$. On the other hand, the magnetic charge is always an integer, and a magnetic charge m sitting at point $\vec{r}$ corresponds to the defect of $\varphi \to \varphi + 2\pi m$ of the bosonic field along a closed contour encircling $\vec{r}$.

The parafermionic operator ϕ_0, for instance, has charges $e = 1 + i\eta/\pi = g$ and $m = 1$, which indeed gives conformal dimensions $\Delta = g = s_0$ and $\bar{\Delta} = 0$. Similarly, ϕ_1 has $(e, m) = (-g, -1)$, whereas $\bar{\phi}_0$ has $(e, m) = (g, -1)$, and $\bar{\phi}_1$ has $(e, m) = (-g, 1)$.

In the case $\eta = 0$, $\phi_0(z)$ and $\phi_1(z)$ are both spin-1 operators and are the $\widehat{\mathfrak{sl}(2)}_1$ lattice operators discussed in [18]. In the continuum limit they scale to the corresponding Wess-Zumino-Witten model currents, which are spin-1 Virasoro primaries [32].

5 Conserved Currents in the SOS Model

In this section we will examine the behaviour of the currents $j_i, \bar{j}_i$ of Section 4 when we dress the boundary of the vertex model with Baxter intertwiners and use the vertex-face correspondence. In this way we will obtain conserved currents in the SOS model.

5.1 Dressed Chevalley generators

Let us define the following functions involving Chevalley generators dressed with our Baxter intertwiners:

$$F_i\left(\begin{array}{cc} a & b \\ & c \end{array}\middle|\,\lambda\right) = \psi^*(a,c|\lambda) f_i\,\psi(a,b|\lambda)\,, \tag{5.1}$$

$$\bar{F}_i\left(\begin{array}{cc} a & b \\ & c \end{array}\middle|\,\lambda\right) = \psi^*(a,c|\lambda) \bar{f}_i\,\psi(a,b|\lambda)\,, \tag{5.2}$$

$$T_i^-\left(\begin{array}{cc} a & b \\ d & c \end{array}\middle|\,\lambda\right) = \psi^*(d,c|\lambda)\, t_i^{-1}\psi(a,b|\lambda)\,, \tag{5.3}$$

$$T_i^+\left(\begin{array}{cc} a & b \\ d & c \end{array}\middle|\,\lambda\right) = \psi'(d,c|\lambda)\, t_i\,\psi(a,b|\lambda)\,. \tag{5.4}$$

Here, we are viewing $\psi(a,b|\lambda)$ as an element of V_λ, and $\psi^*(a,b|\lambda), \psi'(a,b|\lambda) : V_\lambda \to \mathbb{C}$, with the Chevalley generators acting on the representation V_λ as specified in (4.4) and (4.7). Graphically,

we have

$$F_i\left(\begin{matrix} a & b \\ & c \end{matrix}\middle|\,\lambda\right), \quad \bar{F}_i\left(\begin{matrix} a & b \\ & c \end{matrix}\middle|\,\lambda\right) =$$

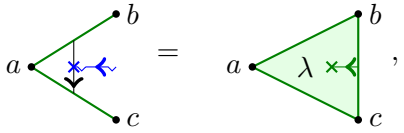

$$T_i^-\left(\begin{matrix} a & b \\ d & c \end{matrix}\middle|\,\lambda\right) =$$

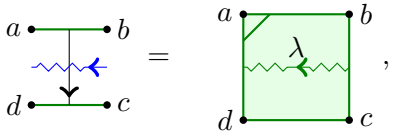

$$T_i^+\left(\begin{matrix} a & b \\ d & c \end{matrix}\middle|\,\lambda\right) =$$

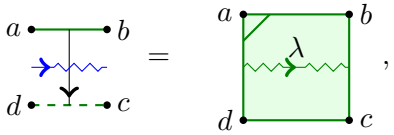

where the pictures in the first column are 'constructive', in the sense that they follow purely from definitions (5.1–5.4) and our previous graphical notations. It is also useful to introduce the second column of representations, in which we now view the objects as new SOS weights. The following explicit expressions follow from definitions (5.1–5.4):

$$F_0\left(\begin{matrix} a & a\pm 1 \\ & a\pm 1 \end{matrix}\middle|\,\lambda\right) = \frac{\pm 1}{2\sinh a\eta}, \qquad F_0\left(\begin{matrix} a & a\mp 1 \\ & a\pm 1 \end{matrix}\middle|\,\lambda\right) = \frac{\pm e^{\pm a\eta}}{2\sinh a\eta}, \tag{5.5}$$

$$F_1\left(\begin{matrix} a & a\pm 1 \\ & a\pm 1 \end{matrix}\middle|\,\lambda\right) = \frac{\mp e^{-2\lambda}}{2\sinh a\eta}, \qquad F_1\left(\begin{matrix} a & a\mp 1 \\ & a\pm 1 \end{matrix}\middle|\,\lambda\right) = \frac{\mp e^{-2\lambda\mp a\eta}}{2\sinh a\eta}, \tag{5.6}$$

$$\bar{F}_0\left(\begin{matrix} a & b \\ & c \end{matrix}\middle|\,\lambda\right) = e^{2\lambda+\eta}F_1\left(\begin{matrix} a & b \\ & c \end{matrix}\middle|\,\lambda\right), \qquad \bar{F}_1\left(\begin{matrix} a & b \\ & c \end{matrix}\middle|\,\lambda\right) = e^{2\lambda+\eta}F_0\left(\begin{matrix} a & b \\ & c \end{matrix}\middle|\,\lambda\right), \tag{5.7}$$

and

$$T_i^-\left(\begin{matrix} a & a\pm 1 \\ d & d\pm 1 \end{matrix}\middle|\,\lambda\right) = \frac{\sinh\frac{(d+a\pm 2\mu_i)\eta}{2}}{\sinh d\eta}, \qquad T_i^-\left(\begin{matrix} a & a\mp 1 \\ d & d\pm 1 \end{matrix}\middle|\,\lambda\right) = \frac{\sinh\frac{(d-a\pm 2\mu_i)\eta}{2}}{\sinh d\eta}, \tag{5.8}$$

where $\mu_0 = 1$ and $\mu_1 = -1$. The functions T_i^+ and T_i^- are related by

$$T_i^+\left(\begin{matrix} a & b \\ d & c \end{matrix}\middle|\,\lambda\right) = T_i^-\left(\begin{matrix} b & a \\ c & d \end{matrix}\middle|\,\lambda\right). \tag{5.9}$$

5.2 Elementary moves of SOS tail operators

Let us now list the properties of these SOS versions of Chevalley generators. First of all, they obey relations which are the analogue of the intertwining condition (4.5). We have

$$\begin{aligned} &\sum_g W\left(\begin{matrix} f & g \\ e & d \end{matrix}\middle|\,\lambda_{12}\right) T_i^-\left(\begin{matrix} a & b \\ f & g \end{matrix}\middle|\,\lambda_1\right) T_i^-\left(\begin{matrix} b & c \\ g & d \end{matrix}\middle|\,\lambda_2\right) \\ &= \sum_g T_i^-\left(\begin{matrix} a & g \\ f & e \end{matrix}\middle|\,\lambda_2\right) T_i^-\left(\begin{matrix} g & c \\ e & d \end{matrix}\middle|\,\lambda_1\right) W\left(\begin{matrix} a & b \\ g & c \end{matrix}\middle|\,\lambda_{12}\right), \end{aligned} \tag{5.10}$$

$$\begin{aligned} &\sum_g W\left(\begin{matrix} f & g \\ e & d \end{matrix}\middle|\,\lambda_{12}\right) T_i^+\left(\begin{matrix} a & b \\ f & g \end{matrix}\middle|\,\lambda_1\right) T_i^+\left(\begin{matrix} b & c \\ g & d \end{matrix}\middle|\,\lambda_2\right) \\ &= \sum_g T_i^+\left(\begin{matrix} a & g \\ f & e \end{matrix}\middle|\,\lambda_2\right) T_i^+\left(\begin{matrix} g & c \\ e & d \end{matrix}\middle|\,\lambda_1\right) W\left(\begin{matrix} a & b \\ c & g \end{matrix}\middle|\,\lambda_{12}\right), \end{aligned} \tag{5.11}$$

which may be drawn as

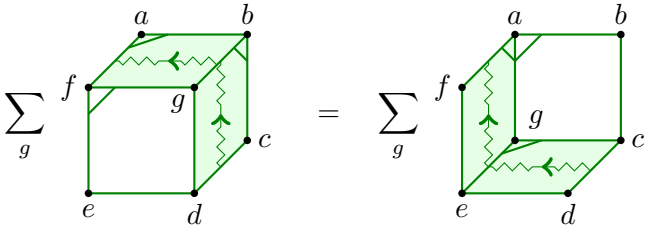

(5.12)

and

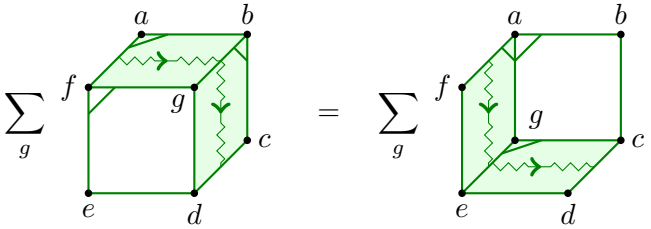

(5.13)

The following inversion relations follow from the corresponding relations (3.12):

$$\sum_e T_i^+ \left(\begin{matrix} d & e \\ c & a \end{matrix} \middle| \lambda \right) T_i^- \left(\begin{matrix} b & a \\ d & e \end{matrix} \middle| \lambda \right) = \delta_{bc} \,, \tag{5.14a}$$

$$\sum_e \frac{\sinh e\eta}{\sinh a\eta} T_i^- \left(\begin{matrix} d & e \\ c & a \end{matrix} \middle| \lambda \right) T_i^+ \left(\begin{matrix} b & a \\ d & e \end{matrix} \middle| \lambda \right) = \frac{\sinh d\eta}{\sinh b\eta} \delta_{bc} \,, \tag{5.14b}$$

$$\sum_e T_i^- \left(\begin{matrix} e & d \\ a & c \end{matrix} \middle| \lambda \right) T_i^+ \left(\begin{matrix} a & b \\ e & d \end{matrix} \middle| \lambda \right) = \delta_{bc} \,, \tag{5.14c}$$

$$\sum_e \frac{\sinh e\eta}{\sinh a\eta} T_i^+ \left(\begin{matrix} e & d \\ a & c \end{matrix} \middle| \lambda \right) T_i^- \left(\begin{matrix} a & b \\ e & d \end{matrix} \middle| \lambda \right) = \frac{\sinh d\eta}{\sinh b\eta} \delta_{bc} \,. \tag{5.14d}$$

The diagrammatic realisation of these four relations will prove useful in later discussions. They are respectively

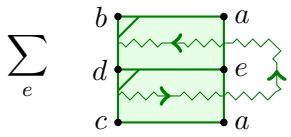

(5.15a)

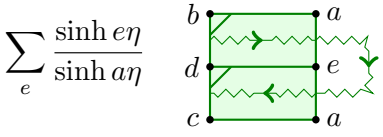

(5.15b)

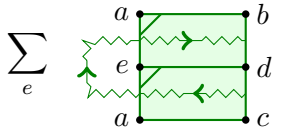

(5.15c)

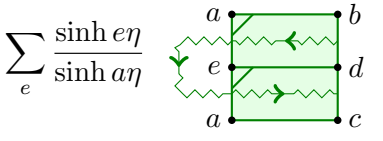

(5.15d)

Finally, we have the relations which are the analogues of the defining relations (4.8) of the

original $U_q(\widehat{\mathfrak{sl}}_2)$ Chevalley generators:

$$\sum_{d,e} \frac{\sinh d\eta}{\sinh a\eta}\, T_i^+ \left(\begin{matrix} d & e \\ a & c \end{matrix} \middle| \lambda \right) F_i \left(\begin{matrix} d & c \\ e & \end{matrix} \middle| \lambda \right) T_i^- \left(\begin{matrix} a & b \\ d & c \end{matrix} \middle| \lambda \right) = e^{2(1-\mu_i)\eta}\, F_i \left(\begin{matrix} a & b \\ c & \end{matrix} \middle| \lambda \right), \tag{5.16}$$

$$\sum_{d,e} \frac{\sinh e\eta}{\sinh b\eta}\, T_i^- \left(\begin{matrix} d & b \\ a & c \end{matrix} \middle| \lambda \right) F_i \left(\begin{matrix} d & e \\ b & \end{matrix} \middle| \lambda \right) T_i^+ \left(\begin{matrix} a & b \\ d & e \end{matrix} \middle| \lambda \right) = e^{2(\mu_i-1)\eta}\, F_i \left(\begin{matrix} a & b \\ c & \end{matrix} \middle| \lambda \right), \tag{5.17}$$

$$\sum_{d,e} \frac{\sinh d\eta}{\sinh a\eta}\, T_i^+ \left(\begin{matrix} d & e \\ a & c \end{matrix} \middle| \lambda \right) \bar{F}_i \left(\begin{matrix} d & c \\ e & \end{matrix} \middle| \lambda \right) T_i^- \left(\begin{matrix} a & b \\ d & c \end{matrix} \middle| \lambda \right) = e^{2(\mu_i-1)\eta}\, \bar{F}_i \left(\begin{matrix} a & b \\ c & \end{matrix} \middle| \lambda \right), \tag{5.18}$$

$$\sum_{d,e} \frac{\sinh e\eta}{\sinh b\eta}\, T_i^- \left(\begin{matrix} d & b \\ a & c \end{matrix} \middle| \lambda \right) \bar{F}_i \left(\begin{matrix} d & e \\ b & \end{matrix} \middle| \lambda \right) T_i^+ \left(\begin{matrix} a & b \\ d & e \end{matrix} \middle| \lambda \right) = e^{2(1-\mu_i)\eta}\, \bar{F}_i \left(\begin{matrix} a & b \\ c & \end{matrix} \middle| \lambda \right), \tag{5.19}$$

where we have set $\mu_0 = 1$ and $\mu_1 = -1$ as in Section 5.1. Note the change from $e^{\pm 2\eta}$ to $\{1, e^{\pm 4\eta}\}$ factors on the right-hand side when compared with (4.8). The diagrammatic versions of (5.16–5.17) are:

$$\sum_{d,e} \frac{\sinh d\eta}{\sinh a\eta}$$

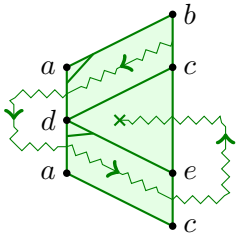

$$= \quad e^{2(1-\mu_i)\eta}$$

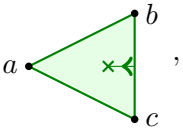

, (5.20)

$$\sum_{d,e} \frac{\sinh d\eta}{\sinh a\eta}$$

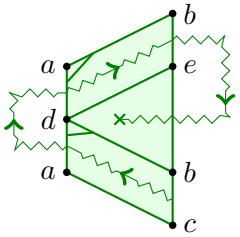

$$= \quad e^{2(\mu_i-1)\eta}$$

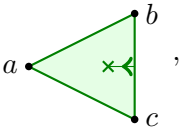

, (5.21)

and similarly for (5.18–5.19), with inverse phase factors on the right-hand side.

5.2.1 Generalised SOS tail operators

It is worth noting that all the elementary moves described so far in Section 5.2 are also satisfied by a larger class of face weights for tails:

$$\tau_\mu^- \left(\begin{matrix} a & b \\ d & c \end{matrix} \middle| \lambda \right) = \psi^*(d,c|\lambda) \begin{pmatrix} e^{+\mu\eta} & 0 \\ 0 & e^{-\mu\eta} \end{pmatrix} \psi(a,b|\lambda)\,, \tag{5.22}$$

$$\tau_\mu^+ \left(\begin{matrix} a & b \\ d & c \end{matrix} \middle| \lambda \right) = \psi'(d,c|\lambda) \begin{pmatrix} e^{-\mu\eta} & 0 \\ 0 & e^{+\mu\eta} \end{pmatrix} \psi(a,b|\lambda)\,, \tag{5.23}$$

for any $\mu \in \mathbb{C}$. The dressed generators $T_0^\pm$ and $T_1^\pm$ simply correspond to $\mu = 1$ and $\mu = -1$ respectively (see Section 5.1).

5.3 Basic four-term relations

The face weights F_i and $T_i^\pm$ obey four-term relations:

$$\sum_g W\left(\begin{matrix} a & g \\ e & d \end{matrix}\middle|\lambda_{12}\right) F_i\left(\begin{matrix} a & b \\ g & \end{matrix}\middle|\lambda_1\right) T_i^-\left(\begin{matrix} b & c \\ g & d \end{matrix}\middle|\lambda_2\right) + W\left(\begin{matrix} a & b \\ e & d \end{matrix}\middle|\lambda_{12}\right) F_i\left(\begin{matrix} b & c \\ & d \end{matrix}\middle|\lambda_2\right)$$
$$= \sum_g F_i\left(\begin{matrix} a & g \\ & e \end{matrix}\middle|\lambda_2\right) T_i^-\left(\begin{matrix} g & c \\ e & d \end{matrix}\middle|\lambda_1\right) W\left(\begin{matrix} a & b \\ g & c \end{matrix}\middle|\lambda_{12}\right) + F_i\left(\begin{matrix} e & c \\ & d \end{matrix}\middle|\lambda_1\right) W\left(\begin{matrix} a & b \\ e & c \end{matrix}\middle|\lambda_{12}\right), \quad (5.24)$$

$$\sum_g W\left(\begin{matrix} a & g \\ e & d \end{matrix}\middle|\lambda_{12}\right) \bar{F}_i\left(\begin{matrix} a & b \\ g & \end{matrix}\middle|\lambda_1\right) T_i^-\left(\begin{matrix} b & c \\ g & d \end{matrix}\middle|\lambda_2\right) + W\left(\begin{matrix} a & b \\ e & d \end{matrix}\middle|\lambda_{12}\right) \bar{F}_i\left(\begin{matrix} b & c \\ & d \end{matrix}\middle|\lambda_2\right)$$
$$= \sum_g \bar{F}_i\left(\begin{matrix} a & g \\ & e \end{matrix}\middle|\lambda_2\right) T_i^-\left(\begin{matrix} g & c \\ e & d \end{matrix}\middle|\lambda_1\right) W\left(\begin{matrix} a & b \\ g & c \end{matrix}\middle|\lambda_{12}\right) + \bar{F}_i\left(\begin{matrix} e & c \\ & d \end{matrix}\middle|\lambda_1\right) W\left(\begin{matrix} a & b \\ e & c \end{matrix}\middle|\lambda_{12}\right), \quad (5.25)$$

which may be drawn as

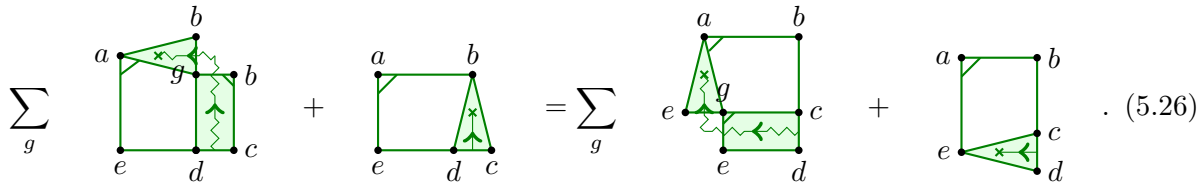

. (5.26)

The proof of these relations follows from the vertex-face correspondence (3.10–3.11), the vertex model intertwining conditions (4.10–4.12), and the inversion relations (3.12a). The proofs are most easily seen diagrammatically. For example, the proof of (5.24) proceeds by the following diagrammatic equalities:

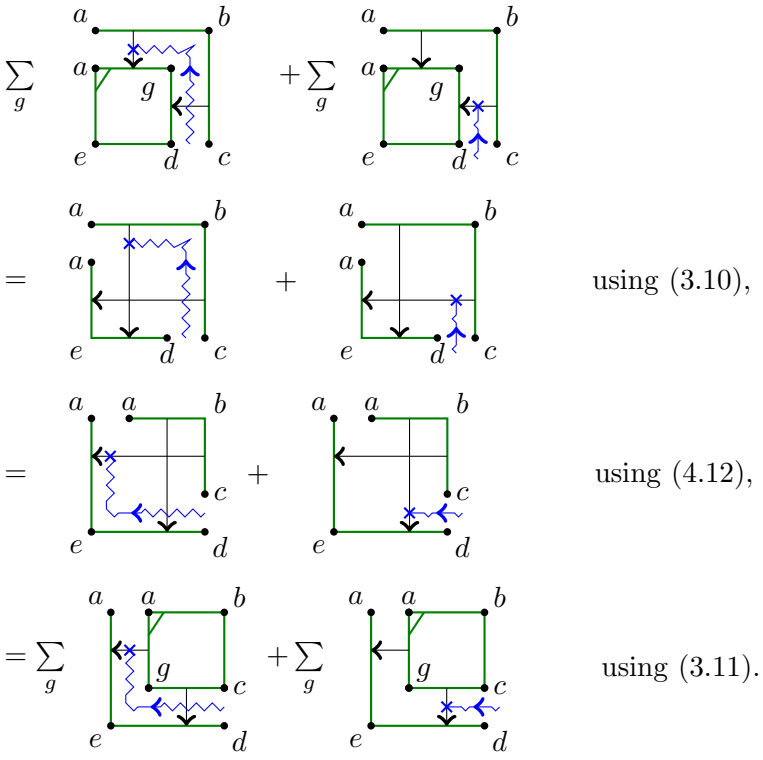

Applying the inversion relation (3.12a) to the right-most term of the first and last lines of this set of equalities leads to the relation (5.24).

5.4 SOS currents

Let us now consider a current insertion in our vertex model with a simple tail configuration of the form of (5.27) below:

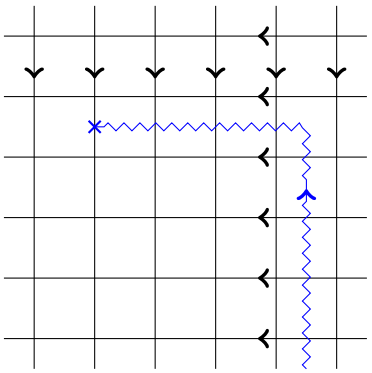

. (5.27)

That is, the tail only travels in a up or left direction from the fixed boundary point to the insertion point. Dressing the boundary[4] and using the vertex-face correspondence, we find

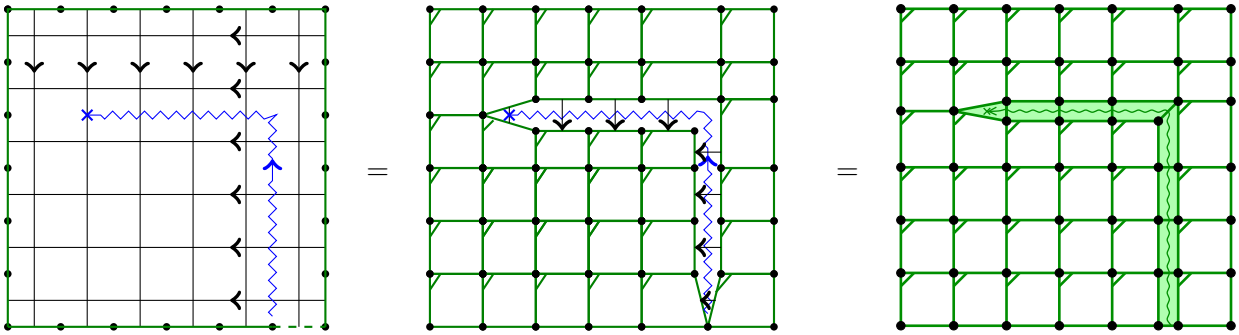

where all internal height variables are summed over (and the boundary heights either side of the insertion point in the final picture are identified). We see that in this example the dressed quasi-local current in the SOS model is made up from a local insertion of F_i or $\bar{F}_i$ and a tail consisting of just T_i^- insertions.

Now suppose we consider general tail configurations corresponding to the f_i or $\bar{f}_i$ currents in our vertex model: these may contain right-going and down-going tails and may have non-trivial winding. Let us define embedded quasi-local SOS currents $J_i(z)$ and $\bar{J}_i(z)$ as consisting of the following (note that after embedding into the complex plane, our SOS lattice squares will appear as tilted rhombi as explained in Section 4.5. For simplicity however, we continue to draw them and describe their orientation in terms of the squares that are their preimage):

- insertion of the operator F_i or $\bar{F}_i$ at embedded lattice point z,
- insertion of left- and up-going portions of tails consisting of $T_i^- =$ as above,
- insertion of right- and down-going portions of tails consisting of $T_i^+ =$,

[4] Note that dressing the bottom right of the boundary with (the dashed) ψ', as opposed to ψ, is just a matter of convenience for this particular tail boundary point; it is useful in order that we can use (3.12c) from the lower right-hand corner.

- insertion of the additional corner factors:

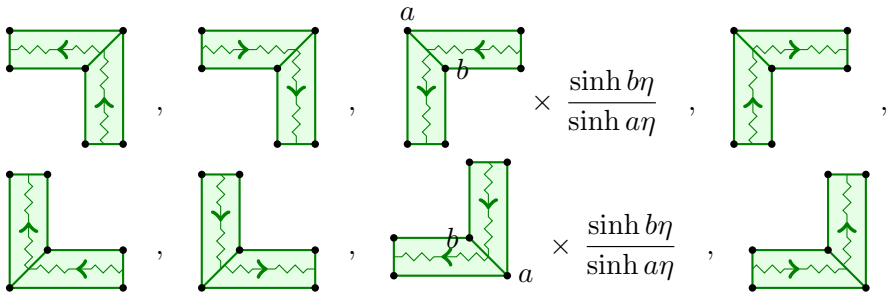

That is, all of the corners are formed from the appropriate pairs of $T_i^{\pm}$ with the additional requirement that the two corners involving left $\to$ down, or down $\to$ left orientations of the tail acquire the extra factor $\frac{\sinh b\eta}{\sinh a\eta}$ indicated depending on the height variables on either side of the corner.

With this definition of SOS currents, we then have the following equivalence under the vertex correspondence

$$j_i(z) \sim e^{2M\mu_i\eta} J_i(z), \quad j_i(z) \sim e^{-2M\mu_i\eta} \bar{J}_i(z)\,, \quad i \in \{0,1\}\,, \tag{5.28}$$

where M is defined to be the anti-clockwise winding number of the tail, and $\mu_0 = 1, \mu_1 = -1$. This equivalence is compatible with the Yang-Baxter relations (5.10–5.11), the inversion inversion relations (5.14a–5.14d), and the commutation relations (5.16–5.19), in the following sense: we can either first move the tail using the corresponding relations for the vertex model as discussed in Section 3, and then apply the vertex-face correspondence, or we can first apply the vertex-face correspondence and then manipulate the SOS tail. The result is the same in both cases.

It also follows from the intertwining relations (5.24–5.25) that $J_i(z)$, $\bar{J}_i(z)$ obey the following four-term current-conservation relation around an SOS plaquette of the form (4.18):

$$J(z_1) - J(z_2) - J(z_3) + J(z_4) = 0\,. \tag{5.29}$$

As always, these relations are to be interpreted as expectation values in the embedded SOS model.

5.5 Parafermionic operators in the SOS Model

We may now proceed as in the vertex model and define

$$\begin{aligned} \Phi_i(z) &= e^{-i\alpha(z)}\, J_i(z)\,, \\ \bar{\Phi}_i(z) &= e^{+i\alpha(z)}\, \bar{J}_i(z)\,, \end{aligned} \tag{5.30}$$

where $\alpha(z)$ has the same definition as in Section 4.5. With these definitions, the SOS current conservation relation (5.29) becomes

$$\delta z_1\, \Phi_i(z_1) + \delta z_2\, \Phi_i(z_2) + \delta z_3\, \Phi_i(z_3) + \delta z_4\, \Phi_i(z_4) \quad = 0\,, \tag{5.31}$$

$$\overline{\delta z}_1\, \bar{\Phi}_i(z_1) + \overline{\delta z}_2\, \bar{\Phi}_i(z_2) + \overline{\delta z}_3\, \bar{\Phi}_i(z_3) + \overline{\delta z}_4\, \bar{\Phi}_i(z_4) \quad = 0\,. \tag{5.32}$$

As with vertex models we can rewrite these expressions in a form where all the spectral-parameter dependence of F_i and $\bar{F}_i$ of equations (5.5–5.7) is taken into an exponential prefactor. Explicitly, we have

$$\Phi_i(z) = e^{-is_i\alpha(z)}\, \mathcal{J}_i(z)\,, \tag{5.33}$$

$$\bar{\Phi}_i(z) = e^{+is_i\alpha(z)}\, \bar{\mathcal{J}}_i(z)\,, \tag{5.34}$$

where

$$s_0 = 1\,, \qquad s_1 = 1 + \frac{2i\eta}{\pi}\,, \tag{5.35}$$

and

$$\mathcal{J}_i(z) = e^{-\frac{2\eta\alpha(z)\delta_{i,1}}{\pi}} J_i(z), \qquad \bar{\mathcal{J}}_i(z) = e^{\frac{2\eta\alpha(z)\delta_{i,1}}{\pi}} J_i(z)$$

are spectral-parameter independent operators.

5.6 Heights adjacent to the tail

The face weights (5.8) have the properties:

$$T_0^-\left(\begin{matrix} b\pm 1 & b \\ b\mp 1 & b \end{matrix}\middle|\,\lambda\right) = 0\,, \qquad T_1^-\left(\begin{matrix} a\pm 1 & a\pm 2 \\ a\mp 1 & a\mp 2 \end{matrix}\middle|\,\lambda\right) = 0\,. \tag{5.36}$$

Let us first discuss the consequences for the currents $J_0(z)$ and $\bar{J}_0(z)$. We shall reason on a simple tail configuration[5] made only of T_0^-'s as in (5.27). If at any point z' on the path of the tail, the height variables across the path are equal, then this is also the case for all pairs of adjacent height variables, along the portion of the path joining z' to the insertion point z. Since the height variables are indeed equal on either side of the boundary insertion point, it follows that the tail is only made of faces of the form:

$$T_0^-\left(\begin{matrix} a & b \\ a & b \end{matrix}\middle|\,\lambda\right) = \frac{\sinh b\eta}{\sinh a\eta}\,. \tag{5.37}$$

Note that the product of all these factors simplifies, so J_0 and $\bar{J}_0$ finally take a local form in terms of the height variables at the insertion point of F_0 or $\bar{F}_0$:

$$J_0 \propto \frac{F_0\left(\begin{smallmatrix} a & b \\ b & \end{smallmatrix}\middle|\,\lambda\right)}{\sinh b\eta}\,, \tag{5.38}$$

and similarly for $\bar{J}_0$. This locality property is consistent with the fact that Φ_0 and $\bar{\Phi}_0$ have integer internal spin.

For the SOS currents J_1 and $\bar{J}_1$, a similar property propagates along the path, but in the opposite direction, i.e., from the insertion point of F_1 or $\bar{F}_1$ to the boundary. The only allowed faces along the path are of the form $T_1^-\left(\begin{matrix} a & b \\ d & c \end{matrix}\middle|\,\lambda\right)$, where $|a-b|=1$, while $|a-d|$ and $|b-c|$ can only take the values $\{-2,0,+2\}$.

5.7 The RSOS case

In this section, we briefly discuss the compatibility of the vertex-face correspondence with RSOS restriction of the face weights. We consider the case $\eta = i\pi/(p+1)$ and integer $p \geq 3$. In this case, as is well known [24], if we set the reference point x_0 [see Section 3.2.1] to zero, we can consistently restrict the SOS height variables to lie in the interval $\{1, 2 \ldots p\}$; the reason is that $W\left(\begin{matrix} a & a+1 \\ a-1 & a \end{matrix}\middle|\,\lambda\right)$ in (3.9) has a simple zero when $a = p$.

Now consider the vertex-face correspondence (3.8), represented graphically by (3.11). In the situation of interest, we have

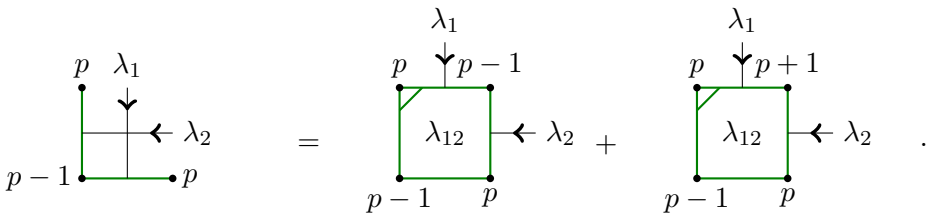

(5.39)

[5] Generic paths may include T_i^+ faces, but the reasoning remains valid, due to the symmetry property (5.9).

Here, both terms on the right-hand-side contribute because the zero in the right-most face weight is cancelled by a pole in the intertwiner $\psi^*(p+1,p|\lambda)$. Nevertheless, if we dress the boundary of the vertex model with intertwiners with heights in $\{1,2,\cdots,p\}$ then it turns out that following the procedure of Section 3.2.2 produces a RSOS partition function with summed over heights purely in the range $\{1,2,\cdots,p\}$ – the reason being that there are further zeros appearing from other products of intertwiners.

However, if we start with a vertex model with current insertions, then it is a simple exercise to check that applying the vertex-face correspondence, as in Section 5.4, produces non-zero weight contributions from configurations with heights outside of $\{1,2,\cdots,p\}$ adjacent to the tail. Thus our current insertions are not compatible with the RSOS restriction, and there is no simple way of understanding the role of our currents in the CFTs associated with RSOS models.

6 The Cyclic Solid-On-Solid model

Throughout this section, we consider the case when η is of the form $\eta = i\pi(p-p')/p$, where p and p' are coprime integers, and $p' < p$.

6.1 The Cyclic SOS Lattice model

Given the two coprime integers p and p', we define the integers ℓ and n as follows:

$$\ell = \begin{cases} \frac{p-p'}{2} & \text{if } (p-p') \text{ is even,} \\ p-p' & \text{if } (p-p') \text{ is odd,} \end{cases} \qquad n = \begin{cases} p & \text{if } (p-p') \text{ is even,} \\ 2p & \text{if } (p-p') \text{ is odd.} \end{cases} \tag{6.1}$$

With this definition, ℓ and n are also coprime, and we have

$$\eta = \frac{i\pi(p-p')}{p} = \frac{2i\pi\ell}{n}\,. \tag{6.2}$$

Then, under a simultaneous shift of all heights, the expressions (3.5–3.6) for Baxter intertwiners $\psi(a,b|\lambda)$ and $\psi^*(a,b|\lambda)$ become n-periodic (resp. antiperiodic) for even ℓ (resp. odd ℓ), and the face weights $W\left(\begin{array}{cc} a & b \\ d & c \end{array}\middle|\lambda\right)$ (3.9) become n-periodic. Hence, one may easily define the analogous objects for heights living in $x_0 + \mathbb{Z}/n\mathbb{Z} \equiv x_0 + \{0,\ldots,n-1\}$. For instance, the definition (3.5) of $\psi(a,a+1)$ is kept for $a \in x_0 + \{0,\ldots,n-2\}$, and completed by:

$$\psi(x_0+(n-1),x_0|\lambda) \equiv \psi(x_0-1,x_0|\lambda) = \begin{bmatrix} \exp\left(\frac{-\lambda+(x_0-1)\eta}{2}\right) \\ \exp\left(\frac{+\lambda-(x_0-1)\eta}{2}\right) \end{bmatrix},$$

and similarly for $\psi(a,a-1|\lambda)$, $\psi^*(a,b|\lambda)$ and $W\left(\begin{array}{cc} a & b \\ d & c \end{array}\middle|\lambda\right)$. In this way, the intertwining relations (3.7–3.8) and the YBE relations (3.13) are transported from the unrestricted SOS model to the cyclic Solid-On-Solid (CSOS) model, i.e., the SOS model with heights living in $x_0 + \mathbb{Z}/n\mathbb{Z}$ and critical weights given by (3.9):

$$\begin{aligned} W\left(\begin{array}{cc} a & a\pm 1 \\ a\pm 1 & a\pm 2 \end{array}\middle|\lambda\right) &= \sinh(\lambda+\eta), \\ W\left(\begin{array}{cc} a & a\pm 1 \\ a\mp 1 & a \end{array}\middle|\lambda\right) &= \frac{\sinh\lambda\ \sinh[(a\pm 1)\eta]}{\sinh(a\eta)}, \\ W\left(\begin{array}{cc} a & a\pm 1 \\ a\pm 1 & a \end{array}\middle|\lambda\right) &= \frac{\sinh\eta\ \sinh(a\eta\mp\lambda)}{\sinh(a\eta)}. \end{aligned}$$

Elliptic CSOS models were introduced and studied in [33–35], and their correlation functions were computed more recently in [36, 37]. Note that in early studies of the CSOS model (see [33–35]), a different limit of the elliptic Boltzmann weights was used, leading to trigonometric weights $W\left(\begin{array}{cc} a & b \\ d & c \end{array}\middle|\lambda\right)$ depending only on differences $(a-b),(b-c),(c-d)$. Here in contrast, we are dealing with *dynamical* trigonometric weights, i.e., the function $W\left(\begin{array}{cc} a & b \\ d & c \end{array}\middle|\lambda\right)$ cannot be expressed solely in terms of $(a-b),(b-c),(c-d)$.

Let us recall the relation to the Temperley-Lieb (TL) loop model [38]. The face weights (3.9) are of the form

$$W\left(\begin{array}{cc} a & b \\ d & c \end{array}\middle|\lambda\right) = \sinh(\lambda+\eta)\,\delta_{bd} + \sinh\lambda\, E\left(\begin{array}{cc} a & b \\ d & c \end{array}\right), \tag{6.3}$$

where

$$E\left(\begin{array}{cc} a & a+\varepsilon_1 \\ a+\varepsilon_2 & b \end{array}\right) = -\varepsilon_1\varepsilon_2\,\delta_{a,b}\frac{\sinh[(a+\varepsilon_1)\eta]}{\sinh[a\eta]}, \quad \varepsilon_1,\varepsilon_2\in\{+,-\}\,. \tag{6.4}$$

The matrix $E\left(\begin{array}{cc} a & b \\ d & c \end{array}\right)$ gives a representation of the generator of the Temperley-Lieb (TL) algebra with loop weight $-2\cosh\eta$.

6.2 Identification of parafermionic operators in the scaling limit CFT

For appropriate boundary conditions, the partition function of the CSOS and TL loop models are equal, and hence their central charges too. For a loop weight $-2\cos\frac{\pi(p-p')}{p}$, Coulomb gas arguments have led to the identification of the TL model central charge as [19, 20]

$$c = 1 - \frac{6(p-p')^2}{pp'}\,. \tag{6.5}$$

A generic method to determine the operator content of SOS models was proposed in [38,39], and was also applied to the 'non-dynamical' critical CSOS model in [35]. Up to our knowledge, this exercise has not been done for the CSOS model with dynamical weights (3.9) that we consider here, and so we have performed it in Appendix A. To summarise, the primary operators are combinations of local height probabilities and height defects, with conformal dimensions

$$\begin{cases} h_{em} = \frac{(ep-mp')^2-(p-p')^2}{4pp'}\,, \\ \\ \bar{h}_{em} = \frac{(ep+mp')^2-(p-p')^2}{4pp'}\,, \end{cases} \qquad e\in\mathbb{Z}/n\,, \quad m\in n\mathbb{Z}\,. \tag{6.6}$$

Our parafermionic operators Φ_0 and $\bar{\Phi}_0$ are local (as shown in Section 5.6) and involve two neighbouring heights (a,b). The construction in Section 5.5 indicates that Φ_0 (resp. $\bar{\Phi}_0$) can be identified with a holomorphic (resp. anti-holomorphic) field of scaling dimension $h=1$ in the continuum limit. This corresponds to the dimension of screening charges, as opposed to conformal primary fields, in the Coulomb Gas picture.

The parafermionic operator Φ_1 is quasi-local, and from Section 5.5 it can be identified with a holomorphic field of scaling dimension $h = s_1 = 1 + 2i\eta/\pi$ (and similarly for $\bar{\Phi}_1$ - which may be identified with an antiholomorphic operator). Using the parametrization (6.6), we find that $s_1 = h_{13}$, and hence identify Φ_1 with the holomorphic part of the degenerate operator Φ_{13}.

7 Conclusions

In this paper, we have used the quantum-group current formalism of [18] in order to construct quasi-local operators in the 6V and trigonometric SOS models. For the 6V case, we have described a systematic procedure that starts from the quantum-group conserved currents and arrives at lattice parafermionic operators (4.24) and (4.25) that (i) obey the discrete integral conditions (4.22) and (4.23) around a rhombus in the complex plane, and (ii) have spins given by (4.26). These spins appear naturally in (4.24) and (4.25) and express the dependence of the operators on the embedding angle shown in (4.16). The identification with CFT primary fields is then automatic and is described in Section 4.6.

For the trigonometric SOS case, we have defined currents of the SOS model as the image of those in the 6V model under the vertex-face correspondence. The resulting quasi-local SOS operators are shown to obey analogous properties to those of the 6V model: for example, the SOS tail can be moved by (5.12) and (5.13), and the currents obey the four-term relation (5.26). Following a very similar procedure to the 6V case, we obtain SOS parafermionic operators obeying the discrete integral conditions (5.31) and (5.32) with spins given by (5.35).

In considering the CFT interpretation of our SOS parafermionic operators, we have concentrated on the CSOS case corresponding to the choice of anisotropy parameter $\eta = i\pi(p-p')/p$, with $p' < p$ coprime. The CSOS case has the twin advantages that it has a relatively well understood CFT limit, and that our quasi-local operators are compatible with the cyclic restriction of height variables (unlike the case for RSOS models as we point out in Section 5.7). We show that our operator Φ_0 actually becomes local in this CSOS case, and we identify it with a CFT screening operator. The operator Φ_1 is still genuinely quasi-local in the CSOS case and is identified with the chiral Φ_{13} operator.

There are various questions that are still under investigation by the authors. One problem is to reinterpret the discrete integral conditions away from the critical line by using perturbed conformal field theory, and to identify perturbing fields. Such an analysis was carried out successfully for the chiral Potts model in [15]; however, the situation for the 6V model close to $\eta = 0$ is more subtle due to the marginal nature of the perturbation associated to the parameter η. Finally, the important question of whether our approach can be extended in certain models in order to produce fully discretely-holomorphic operators, whose existence would pave the way for rigorous results on the scaling limit, remains open.

Acknowledgements

We would like to thank Benoît Estienne, Nikolai Kitanine, Véronique Terras and Paul Zinn-Justin for sharing their useful insights and advice. We also acknowledge the support and hospitality of the Galileo Galilei Institute for Theoretical Physics, and the organisers of the Statistical Mechanics, Integrability and Combinatorics workshop at which this work was begun. RAW would like to thank the Laboratoire de Physique Théorique et Hautes Energies (Université Pierre et Marie Curie/CNRS) for providing warm hospitality and funding during several visits to Paris.

References

[1] A. A. Belavin, A. M. Polyakov, and A. B. Zamolodchikov. Infinite conformal symmetry in two-dimensional quantum field theory. *Nuclear Phys. B*, 241(2):333–380, 1984.

[2] R. Kenyon. Dominos and the Gaussian free field. *Ann. Probab.*, 29(3):1128–1137, 2001.

[3] S. Smirnov. Conformal invariance in random cluster models. I. Holomorphic fermions in the Ising model. *Ann. of Math. (2)*, 172(2):1435–1467, 2010.

[4] D. Chelkak and S. Smirnov. Universality in the 2D Ising model and conformal invariance of fermionic observables. *Invent. Math.*, 189(3):515–580, 2012.

[5] S. Smirnov. Critical percolation and conformal invariance. In *XIVth International Congress on Mathematical Physics*, pages 99–112. World Sci. Publ., Hackensack, NJ, 2005.

[6] S. Smirnov. Critical percolation in the plane: conformal invariance, Cardy's formula, scaling limits. *C. R. Acad. Sci. Paris Sér. I Math.*, 333(3):239–244, 2001.

[7] H. Duminil-Copin and S. Smirnov. The connective constant of the honeycomb lattice equals $\sqrt{2+\sqrt{2}}$. *Ann. of Math. (2)*, 175(3):1653–1665, 2012.

[8] S. Smirnov. Discrete complex analysis and probability. In *Proceedings of the International Congress of Mathematicians. Volume I*, pages 595–621, New Delhi, 2010. Hindustan Book Agency.

[9] V. Riva and J. Cardy. Holomorphic parafermions in the Potts model and Stochastic Loewner Evolution. *J. Stat. Mech.*, (12):P12001, 19 pp. (electronic), 2006.

[10] M. A. Rajabpour and J. Cardy. Discretely holomorphic parafermions in lattice Z_N models. *J. Phys. A*, 40(49):14703–14713, 2007.

[11] Y. Ikhlef and M. A. Rajabpour. Discrete holomorphic parafermions in the Ashkin-Teller model and SLE. *J. Phys. A*, 44(4):042001, 11, 2011.

[12] Y. Ikhlef and J. Cardy. Discretely holomorphic parafermions and integrable loop models. *J. Phys. A*, 42(10):102001, 11, 2009.

[13] Y. Ikhlef. Discretely holomorphic parafermions and integrable boundary conditions. *J. Phys. A*, 45(26):265001, 12, 2012.

[14] Y. Ikhlef, R. Weston, M. Wheeler, and P. Zinn-Justin. Discrete holomorphicity and quantized affine algebras. *J. Phys. A*, 46(26):265205, 34, 2013.

[15] Y. Ikhlef and R. Weston. Discrete holomorphicity in the chiral Potts model. *J. Phys. A*, 48(29):294001, 24, 2015.

[16] J. de Gier, A. Lee, and J. Rasmussen. Discrete holomorphicity and integrability in loop models with open boundaries. *J. Stat. Mech. Theory Exp.*, (2):P02029, 27, 2013.

[17] I. T. Alam and M. T. Batchelor. Integrability as a consequence of discrete holomorphicity: the $\mathbf{Z}_N$ model. *J. Phys. A*, 45(49):494014, 10, 2012.

[18] D. Bernard and G. Felder. Quantum group symmetries in two-dimensional lattice quantum field theory. *Nucl. Phys. B*, 365(1):98–120, 1991.

[19] B. Nienhuis. Critical behavior of two-dimensional spin models and charge asymmetry in the Coulomb gas. *J. Stat. Phys.*, 34(5-6):731–761, 1984.

[20] B. Nienhuis. Exact critical point and critical exponents of O(n) models in two dimensions. *Phys. Rev. Lett.*, 49(15):1062–1065, 1982.

[21] J. L. Cardy. Critical exponents of the chiral Potts model from Conformal Field Theory. *Nucl. Phys. B*, 389:577–586, 1993.

[22] M. Jimbo, H. Konno, S. Odake, and J. Shiraishi. Quasi-Hopf twistors for elliptic quantum groups. *Transform. Groups*, 4(4):303–327, 1999.

[23] R. J. Baxter. Eight-Vertex Model in Lattice Statistics and One-Dimenisional Anisotropic Heisenberg Chain. 11. Equivalence to a Generalized Ice-type Model. *Annals of Physics*, 76:25–47, 1973.

[24] G. E. Andrews, R. J. Baxter, and P. J. Forrester. Eight-vertex SOS model and generalized Rogers-Ramanujan-type identities. *J. Stat. Phys.*, 35:193–266, 1984.

[25] G. Filali and N. Kitanine. The partition function of the trigonometric SOS model with a reflecting end. *J. Stat. Mech. Theory Exp.*, (6):L06001, 11, 2010.

[26] E. Date, M. Jimbo, T. Miwa, and M. Okado. Fusion of the eight vertex SOS model. *Lett. Math. Phys.*, 12(3):209–215, 1986.

[27] G. Felder. Elliptic quantum groups. In *XIth International Congress of Mathematical Physics (Paris, 1994)*, pages 211–218. Int. Press, Cambridge, MA, 1995.

[28] T. Kojima, H. Konno, and R. Weston. The vertex-face correspondence and correlation functions of the fusion eight-vertex model. I. The general formalism. *Nuclear Phys. B*, 720(3):348–398, 2005.

[29] M. Lashkevich and Y. Pugai. Free field construction for correlation functions of the eight-vertex model. *Nuclear Phys. B*, 516(3):623–651, 1998.

[30] M. Jimbo. Topics from representations of $U_q(\mathfrak{g})$—an introductory guide to physicists. In *Quantum group and quantum integrable systems*, Nankai Lectures Math. Phys., pages 1–61. World Sci. Publ., River Edge, NJ, 1992.

[31] P. Di Francesco, H. Saleur, and J.-B. Zuber. Relations between the Coulomb gas picture and conformal invariance of two-dimensional critical models. *J. Statist. Phys.*, 49(1-2):57–79, 1987.

[32] P. Di Francesco, P. Mathieu, and D. Sénéchal. *Conformal field theory*. Graduate Texts in Contemporary Physics. Springer-Verlag, New York, 1997.

[33] A. Kuniba and T. Yajima. Local state probabilities for solvable restricted solid-on-solid models: A_n, D_n, $D_n^{(1)}$, and $A_n^{(1)}$. *J. Statist. Phys.*, 52(3-4):829–883, 1988.

[34] P. A. Pearce and K. A. Seaton. Exact solution of cyclic solid-on-solid lattice models. *Ann. Physics*, 193(2):326–366, 1989.

[35] D. Kim and P. A. Pearce. Operator content of the cyclic solid-on-solid models. *J. Phys. A*, 22(9):1439–1450, 1989.

[36] D. Levy-Bencheton and V. Terras. Multi-point local height probabilities of the CSOS model within the algebraic Bethe ansatz framework. *J. Stat. Mech. Theory Exp.*, (4):P04014, 45, 2014.

[37] D. Levy-Bencheton and V. Terras. An algebraic Bethe ansatz approach to form factors and correlation functions of the cyclic eight-vertex solid-on-solid model. *J. Stat. Mech. Theory Exp.*, (4):P04015, 37, 2013.

[38] V. Pasquier. Lattice derivation of modular invariant partition functions on the torus. *J. Phys. A*, 20(18):L1229–L1237, 1987.

[39] V. Pasquier. Operator content of the ADE lattice models. *J. Phys. A*, 20(16):5707–5717, 1987.

A Operator content in the Scaling Limit of the CSOS Model

A.1 Local height probabilities

In this appendix, we sketch the analysis of local operators in the critical CSOS model, using the approach of [39]. The CSOS model with heights in $x_0 + \mathbb{Z}/n\mathbb{Z}$ and weights (3.9) corresponds to the adjacency matrix

$$A_{ab} = \begin{cases} 1 & \text{if } |a-b| \equiv 1 \mod n\,, \\ 0 & \text{otherwise.} \end{cases} \tag{A.1}$$

We consider n orthonormal eigenvectors of A, which we denote by

$$\{S^{(1)}, \cdots, S^{((n-1)/2)}, T^{(0)}, T^{(1)}, \cdots T^{((n-1)/2)}\} \qquad \text{for odd } n, \tag{A.2}$$

$$\{S^{(1)}, \cdots, S^{(n/2-1)}, T^{(0)}, T^{(1)}, \cdots T^{(n/2)}\} \qquad \text{for even } n. \tag{A.3}$$

Components are given by

$$S_a^{(j)} = N_j \sin\left(\frac{2\pi a j}{n}\right), \qquad T_a^{(j)} = N_j \cos\left(\frac{2\pi a j}{n}\right), \quad a \in \{0, 1, \cdots, n-1\}\,, \tag{A.4}$$

where $N_j = \sqrt{1/n}$ if $j = 0$ or $j = n/2$, and $N_j = \sqrt{2/n}$ otherwise. Let us define (for the appropriate range of j for n odd or even)

$$\varphi_a^{(j)} = \frac{S_a^{(j)}}{S_a^{(\ell)}}\,, \qquad \psi_a^{(j)} = \frac{T_a^{(j)}}{S_a^{(\ell)}}\,, \tag{A.5}$$

where ℓ is defined by (6.1). Local operators, which we denote by the same notation $\varphi_a^{(j)}$ and $\psi_a^{(j)}$, have the following effect in the TL graphical expansion [39]: any loop enclosing a single operator $\varphi_a^{(j)}$ or $\psi_a^{(j)}$ is assigned a weight $-2\cos\frac{2\pi j}{n}$ instead of $-2\cos\frac{2\pi\ell}{n} = -2\cosh\eta$. The difference between $\varphi_a^{(j)}$ or $\psi_a^{(j)}$ appears when a loop encloses a product of operators, which is important for multi-point correlation functions. We shall not discuss this further, since the two-point functions are enough for the determination of critical exponents.

Using standard Coulomb gas arguments for the loop model [19], one can identify $\varphi_a^{(j)}$ or $\psi_a^{(j)}$ as an electric charge $e = 2j/n + k$, where $k \in \mathbb{Z}$, and the corresponding conformal dimensions are given by:

$$h = \bar{h} = \frac{(2j/n + k)^2}{4p'/p} - \frac{(p-p')^2}{4pp'}\,. \tag{A.6}$$

From the relation (6.1) between n and (p, p'), it is clear that the electric charge $e = 2j/n + k$ spans $\mathbb{Z}/n$ as j ranges from 0 to $(n-1)$ and $k \in \mathbb{Z}$. Note also that some of these exponents are negative: in particular, the operator $\psi_a^{(0)}$ has electric charge $e = 0$ and dimension $h_0 = \bar{h}_0 = -\frac{(p-p')^2}{4pp'} < 0$, which yields the effective central charge $c_{\text{eff}} = c - 12(h_0 + \bar{h}_0) = 1$. In contrast, the identity operator $\varphi_a^{(\ell)}$ has electric charge $e = 2\ell/n$ and dimensions $h = \bar{h} = 0$.

A.2 Defect operators

Due to the n-periodicity of height variables, the CSOS model also admits some defect operators. For any non-zero integer m, the operator that inserts a height defect $a \to a + mn$ around a given point forces mn segments of loops to join in the vicinity of this point. The corresponding 'magnetic' conformal dimension is

$$h = \bar{h} = \frac{p'}{4p}(mn)^2 - \frac{(p-p')^2}{4pp'}\,. \tag{A.7}$$

Electric and magnetic operators may be combined, leading to a (generally non-scalar) primary operator with dimensions

$$\begin{cases} h_{em} = \frac{(ep-mp')^2-(p-p')^2}{4pp'}\,, \\ \\ \bar{h}_{em} = \frac{(ep+mp')^2-(p-p')^2}{4pp'}\,, \end{cases} \qquad e \in \mathbb{Z}/n\,, \quad m \in n\mathbb{Z}\,. \tag{A.8}$$

A.3 Partition function on the torus

Using the approach of [38], we can map the toroidal partition function of the CSOS model to a linear combination of TL partition functions, which in turn are related to 6V partition functions with proper topological factors [31]. This line of arguments yields the simple result in the scaling limit:

$$Z_{\mathrm{CSOS}}(q) = \frac{(q\bar{q})^{c/24}}{|\eta(q)|^2} \sum_{e\in\mathbb{Z}/n,\, m\in n\mathbb{Z}} q^{h_{em}} \bar{q}^{\bar{h}_{em}}\,. \tag{A.9}$$

where $q = e^{2i\pi\tau}$, τ is the modular parameter, and η is the Dedekind eta function. This expression is consistent with the interpretation of the CSOS model as a CFT with central charge (6.5) and operator content (A.8).